

Control of emission interval and timing in triggered periodic superradiance

Hideaki Hara^{*1}, Riku Omoto¹, Noboru Sasao¹, Akihiro Yoshimi¹,
Junseok Han^{1,2}, Yasutaka Imai¹, Koji Yoshimura¹,
Motohiko Yoshimura¹, and Yuki Miyamoto^{†1}

¹*Research Institute for Interdisciplinary Science, Okayama University, Okayama, 700-8530, Japan*

²*Department of Physics and Astronomy, Seoul National University, Seoul, Korea*

March 30, 2026

Abstract

To achieve more controllable development of coherence in solids, we investigated the effect of a trigger laser tuned to the superradiance transition wavelength on periodic superradiance observed in an Er:YSO crystal. For period control, applying the trigger laser reduced both the superradiance period and its variance, demonstrating enhanced controllability of coherence development dynamics. As the trigger laser power increased, both the period and the number of emitted superradiance photons decreased while maintaining a proportional relationship. This behavior is explained by a reduced superradiance threshold under a constant excitation rate and is reproduced by numerical simulations based on the Maxwell-Bloch equations. For timing control, we found that superradiance could be triggered even when the excitation laser alone was insufficient. This enabled us to control the emission timing of superradiance using short trigger pulses and provided a device capable of generating superradiance at desired timing.

1 Introduction

Superradiance (SR) has been extensively studied [1–11], and a particular variant, triggered SR, has also attracted attention. In the case of triggered SR, the emission timing

*Email: hhara@okayama-u.ac.jp

†Email: miyamo-y@cc.okayama-u.ac.jp

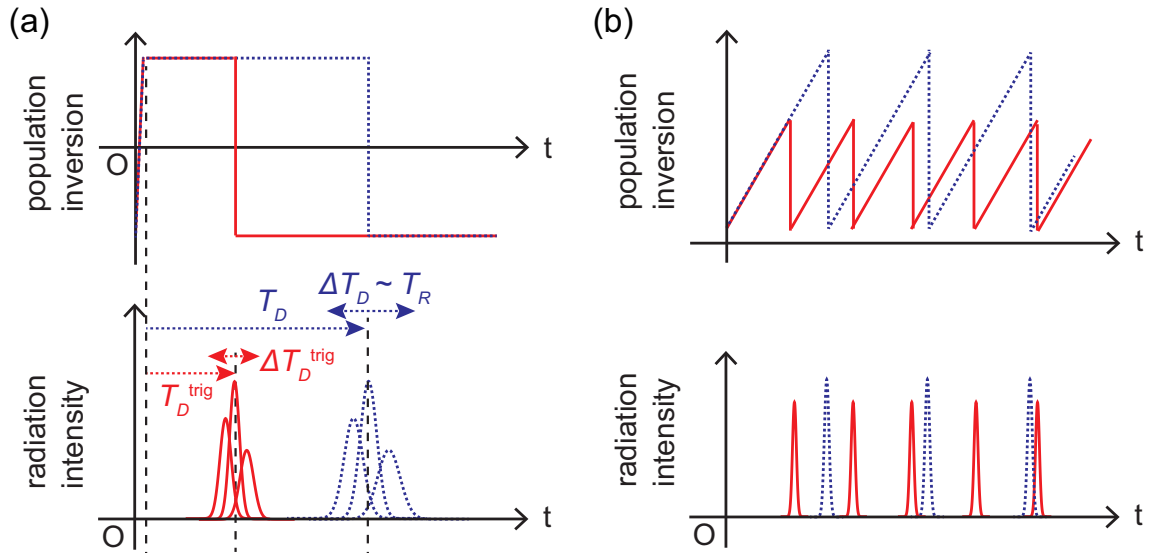


Figure 1: (a) Conceptual illustration of conventional (non-periodic) SR. (Top) Temporal change in the population inversion without (blue dotted line) and with (red solid line) a trigger laser. The initial rapid increase represents excitation by the pump pulse, while the trigger laser—either CW or pulsed—serves as a deterministic seed for coherence development. (Bottom) A single SR pulse is shown, with pulse-to-pulse variation indicated. (b) Conceptual illustration of periodic SR. (Top) Temporal evolution of the population inversion without (blue dotted line) and with (red solid line) a trigger laser. Both the excitation and the trigger laser are CW. (Bottom) Periodic SR pulses are shown.

of SR can be controlled by irradiating a laser at the same wavelength as the SR transition [12]. In general, SR exhibits a delay time (T_D) required for coherence to fully develop after the population inversion is formed as shown by the blue dotted line in Fig. 1 (a). In untriggered SR, coherence emerges from quantum fluctuations, where the electric field of spontaneous emission acts as a seed. Consequently, T_D reflects initial quantum fluctuation and exhibits significant pulse-to-pulse variation (ΔT_D). In triggered SR, by contrast, the external laser field—either continuous-wave (CW) or pulsed—serves as a deterministic seed for coherence development. As a result, T_D^{trig} , the delay time in the presence of a trigger laser, becomes shorter and more stable, with reduced shot-to-shot fluctuations, as shown by the red solid line in Fig. 1 (a). This can be regarded as a clear example of emission timing control in SR. Such timing-controlled SR holds potential for applications in quantum information processing, such as utilizing deexcitation signals for quantum memory readout [13]. Triggered SR also enables strong amplification induced by a trigger laser acting as a weak external input [11, 14]. Moreover, it has been proposed as a possible physical mechanism underlying astrophysical phenomena known as fast radio bursts (FRBs) [15]. Recently, triggered SR has been explored in Rydberg gases, where blackbody radiation induces emission [16]. These studies high-

light a growing interest in externally controlling collective emission process for quantum technologies.

In the long history of research on SR, we recently observed quasiperiodic SR pulses in an Er:YSO crystal under CW laser excitation, without modulation of input parameters. We referred to this phenomenon as “periodic superradiance” [17]. This behavior can be understood as a repeated cycle of population inversion buildup via pumping, followed by a sudden SR burst once the population inversion reaches a certain threshold, as shown in Fig. 1 (b). In this paper, we refer to SR behavior that is not periodic as “conventional SR.” Unlike conventional SR, periodic SR exhibits regular, repeated pulses. The emergence of periodic SR implies partial control of coherence development; indeed, the SR period varies with excitation laser power, though with considerable fluctuation.

Inspired by triggered SR, we hypothesize that applying a trigger laser to a system exhibiting periodic SR provides a deterministic seed, which accelerates coherence development and thereby may shorten the SR period while suppressing its fluctuation (see the red solid line in Fig. 1 (b)). This concept can be referred to as “triggered periodic SR,” which represents a step toward enhanced temporal control of coherence development in solid-state systems. If periodic SR can be stabilized, it may serve as a practical light source producing nanosecond optical pulses. Our previous measurements showed that the linewidth of SR pulses emitted from an Er:YSO crystal was much narrower than the inhomogeneous broadening. Furthermore, precise control of the SR emission timing is equivalent to controlling the moment when the system reaches maximum coherence. Performing other quantum operations at this moment—such as laser-driven manipulations—allows the effects of collective coherence to be fully utilized and enables synchronization with the system’s peak coherence.

In this paper, we begin by investigating the effect of a trigger laser, whose wavelength is tuned to the same wavelength as the SR transition, on the behavior of periodic SR. Specifically, we measure the dependence of periodic SR on the trigger laser power under conditions where periodic SR can occur even without the trigger laser. We extend our previous simulation method for periodic SR [18] to incorporate the effect of the trigger laser and attempt to reproduce the experimentally observed dependence on trigger power. We then examine the role of the trigger laser in conditions where periodic SR does not occur in the absence of the trigger laser. These experiments suggest the possibility of controlling SR emission timing using a short-duration trigger laser pulse and this system can be regarded as a device capable of SR pulse emission at desired timing.

2 Experimental setup

Er³⁺ ions doped at site 2 of a YSO crystal, which is cooled at 4 K, are used in our experiment. The number density of the Er³⁺ ions at site 2 is $5 \times 10^{18} \text{ cm}^{-3}$ according to the nominal concentration value of 0.1%. Figure 2 shows the energy diagram. The difference from the previous experiment [17] is the addition of the trigger laser. The SR pulses with a wavelength of 1545 nm are generated in the transition from the lowest Stark level of the $^4I_{13/2}$ state to the second lowest Stark level of the $^4I_{15/2}$ ground state.

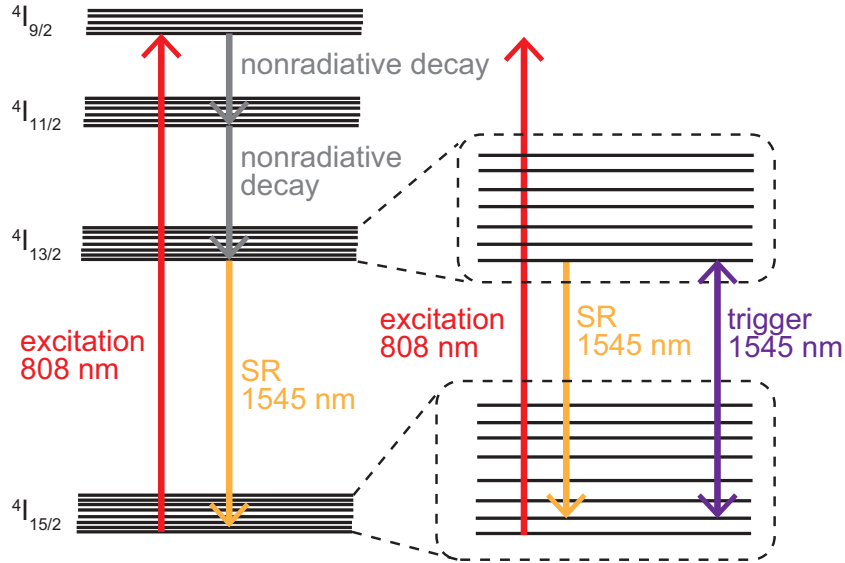


Figure 2: Energy diagram of Er^{3+} ion doped in YSO crystal. The dashed rounded square shows enlarged views of the $4I_{13/2}$ and $4I_{15/2}$ states, respectively.

To trigger the SR pulses, a trigger laser with a wavelength of 1545 nm is injected into the crystal. The wavelength of the trigger laser is tuned to the SR transition wavelength. The excitation and trigger lasers propagate along the b axis of the crystal. Both lasers are loosely focused on the crystal. The beam diameters ($2w_0$) at the crystal are roughly $300 \mu\text{m}$ (excitation) and $450 \mu\text{m}$ (trigger), respectively. The input excitation laser power is typically 60 mW. The trigger laser power is different for each measurement and ranges from $10 \mu\text{W}$ to 9 mW in this paper. The polarization of the excitation laser is parallel to the \mathbf{D}_2 axis of the crystal. The polarization of the SR pulses in the absence of the trigger laser is approximately parallel to the \mathbf{D}_1 axis. The excitation laser is turned on for 40 ms ($t = 0 \sim 40$ ms) every 200 ms. The trigger laser is turned on for the middle 10 ms ($t = 15 \sim 25$ ms) during the excitation. The 40 ms excitation data are taken repeatedly.

3 Results and discussion

3.1 Change in SR period caused by trigger laser

3.1.1 Experimental results

First, we observed that the SR period changed when the trigger laser was irradiated. Figure 3 (a) and (b) show examples of the waveform of observed periodic SR pulses with and without trigger laser irradiation, respectively. In this case, the trigger laser of 0.5 mW is injected. The pulses are generated at almost constant time interval in both cases. When triggered, the peak interval decreases as we expected in Sec.1. Figure 3 (c) shows

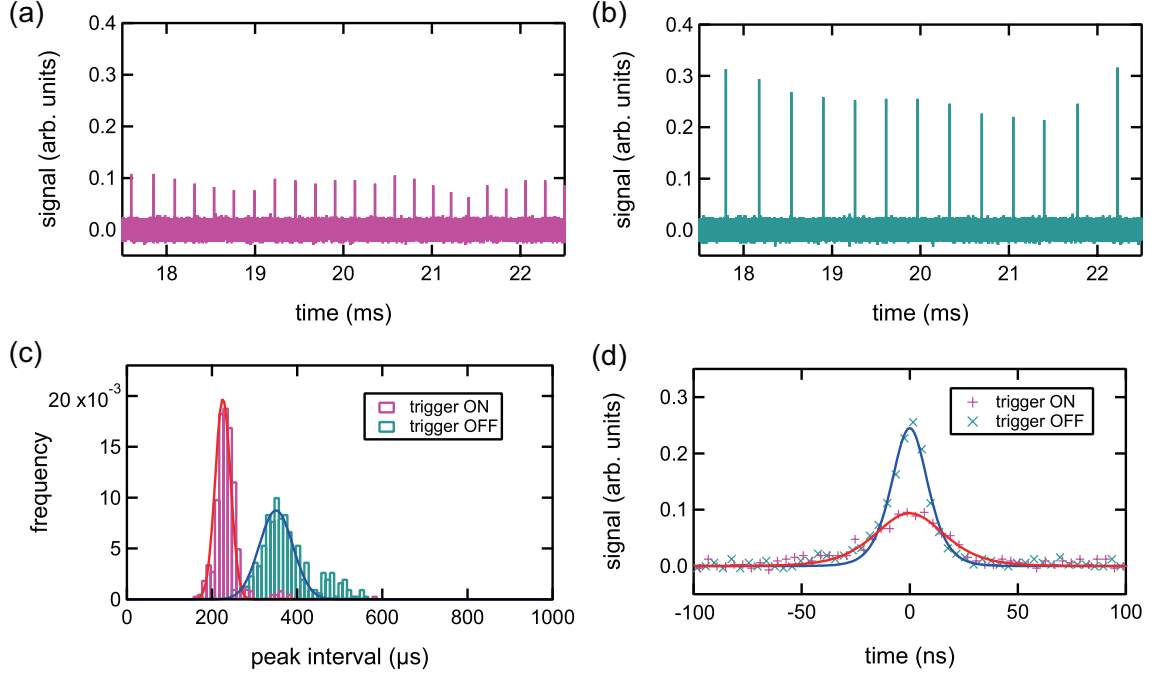


Figure 3: (a) Example of waveform of observed periodic SR pulses with trigger laser irradiation. The excitation laser is turned on for 40 ms from $t = 0$ and the trigger laser is turned on for 10 ms from $t = 15$ ms. (b) Example of waveform of observed periodic SR pulses without trigger laser irradiation. (c) Histograms of the peak interval between neighboring pulses with (magenta) and without (green) trigger laser irradiation. The red and blue lines are the Gaussian fits. The data in the time region of $t = 15 \sim 25$ ms, during which the trigger laser is irradiated, are used for this plot. (d) Examples of observed single SR pulses with (magenta cross) and without (green X) trigger laser irradiation. The red and blue solid lines are the fit by sech-squared functions. Each peak timing is set as the origin of time.

histograms of peak intervals, defined by the time difference between neighboring peaks, with (magenta) and without (green) trigger laser irradiation. It can be clearly seen that the peak interval decreases when the trigger laser is turned on. This is consistent with the intuition that coherence develops faster when the trigger laser is used as a seed rather than spontaneously emitted photons. The period given by the Gaussian fit is $230 \pm 20 \mu\text{s}$ with trigger and $350 \pm 40 \mu\text{s}$ without trigger. The notation here is (center value $\pm 1\sigma$). Both the average value of the period and its variance decrease. This is thought to correspond to the reductions of the delay time and its variance in conventional triggered SR. The decrease in period variability can be interpreted as an improvement in the temporal control of coherence development. In addition to the decrease in period, it can be seen that the pulse height also decreases. Considerations regarding the decrease in pulse height will be discussed in Sec. 3.1.2, which addresses trigger power dependence.

Figure 3 (d) shows examples of single SR pulses with (magenta cross) and without (green X) trigger laser irradiation. The FWHM (full-width-half-maximum) pulse durations are 37 ± 7 ns with trigger and 19 ± 2 ns without trigger, respectively. They are given by the Gaussian fits to the histograms of the duration. In the case of trigger irradiation, the increasing of the pulse duration is consistent with the decreasing of the peak height, and can be understood as conventional SR behavior. The red and blue solid lines are the fits by sech-squared functions. This functional shape can be seen when the coherence develops homogeneously over the target [19] as in our experimental condition. Other properties regarding frequency and polarization are introduced in Appendix (C) and (D).

3.1.2 Trigger power dependence

As shown in Sec. 3.1.1, the trigger laser affects the behavior of periodic SR. Next, we investigate the effect of trigger laser power on periodic SR. Figure 4 (a) shows the peak interval (left axis, red circle) and pulse area (right axis, blue diamond) as functions of the trigger laser power. The leftmost data points correspond to the values without the trigger laser. The vertical axes are normalized such that the period and pulse area without the trigger laser appear at the same height. When the trigger power is sufficiently weak, the peak interval and pulse area remain close to those without trigger laser, indicating that the trigger has a negligible effect in the weak-power limit. Above $10 \mu\text{W}$, both period and pulse area decrease with increasing trigger power, showing that the trigger laser influences the SR behavior in the intermediate power range. Furthermore, the period and the number of emitted SR photons decreases while maintaining a proportional relationship with each other. When the trigger power exceeds 1 mW , SR emission is no longer observed. This may be due to stimulated emission depleting the population of the upper state involved in the SR transition, preventing the population inversion from reaching the threshold required for SR.

The period of SR is shortened by the trigger laser, corresponding to the shorter delay time in conventional triggered SR [12]. The dependence of the pulse area on the trigger laser power can be interpreted by consideration of the threshold condition for SR. For SR to occur, the macroscopic dipole has to develop within a decoherence time T_2 and the population inversion has to reach a certain threshold. That is, $T_D < T_2$ is required. The delay time T_D is related to the characteristic time of SR, which in a simple two-level model is given by [20]

$$T_R = 8\pi/(3\gamma N_0 \lambda^2 L), \quad (1)$$

through the expression $T_D = T_R \ln(N_0 V)$ [21]. Here N_0 is a number density of Er^{3+} ions related to SR, λ is a wavelength of SR (1545 nm), L is a sample length (6 mm), γ is a radiative decay rate, and V is an excitation volume. Defining $f = \ln(N_0 V)$, one finds that f typically takes values on the order of 10. The threshold of the population inversion N_{th} is determined by the above inequality to be $N_{\text{th}} = (8\pi/3\gamma T_2)(V/\lambda^2 L)f$. As shown in Fig. 1 (a), the delay time in the presence of the trigger laser, denoted as T_D^{trig} , is shortened compared to the untriggered case. This can be expressed as $T_D^{\text{trig}} = T_D/p_{\text{trig}}$, where the quantity $p_{\text{trig}} (> 1)$ is a conceptual parameter that expresses how much T_D

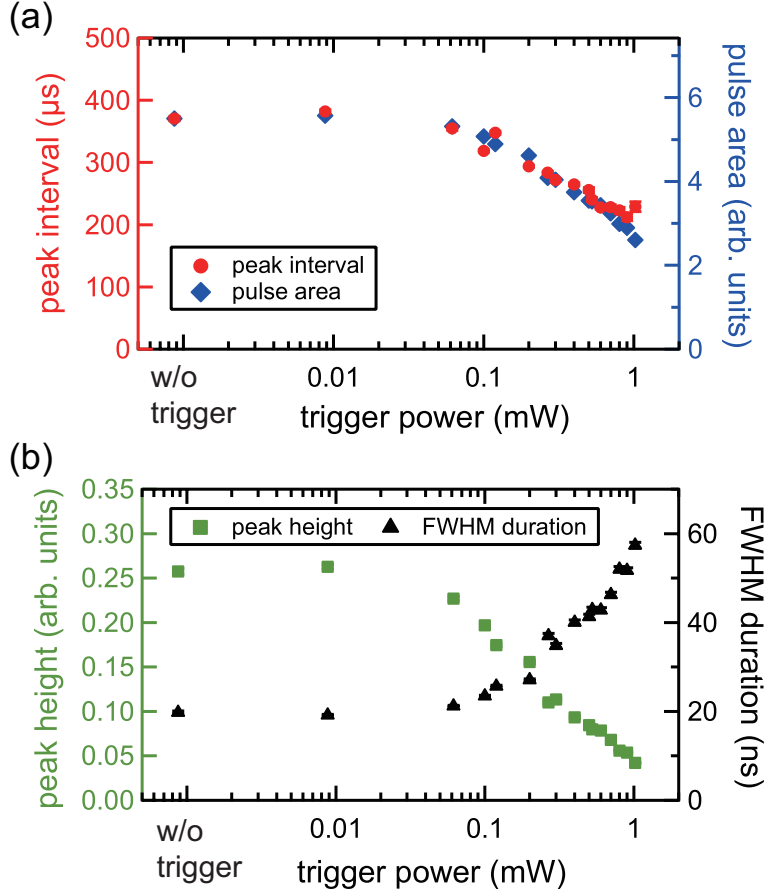


Figure 4: (a) Peak interval (left axis, red circle) and pulse area (right axis, blue diamond) at various trigger laser power. (b) Peak height (left axis, green square) and FWHM pulse duration (right axis, black triangle) at various trigger laser power. The error bars are the standard errors. The leftmost points are the values without the trigger laser.

decreases by the trigger. p_{trig} is equal to unity in the limit of weak trigger laser power, and increases as the trigger power becomes stronger. In the presence of a trigger laser, the requirement for SR is expected to be modified to $T_D^{\text{trig}} < T_2$. The population inversion threshold for SR under the trigger laser, $N_{\text{th}}^{\text{trig}}$, is also reduced as $N_{\text{th}}^{\text{trig}} = N_{\text{th}}/p_{\text{trig}}$. This decrease in threshold leads to a corresponding reduction in the number of emitted SR photons. Since the excitation rate remains constant, the number of SR photons generated during each cycle scales proportionally with the SR period. This situation is conceptually illustrated in Fig. 1 (b, Top). Thus, a proportional relationship exists between the SR period and the number of emitted photons.

Figure 4 (b) shows the peak height (left axis, green square) and FWHM pulse duration (right axis, black triangle), respectively. When the trigger power is low, both values are comparable to those observed without the trigger laser. Above 10 μW , the peak height

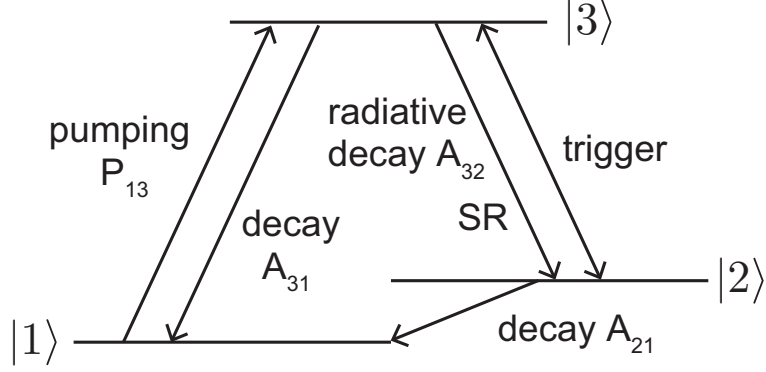


Figure 5: Reduction to extend two-level system in our model. The states $|1\rangle$ and $|2\rangle$ correspond to the lowest and second lowest Stark levels of the ${}^4I_{15/2}$ ground state, respectively. The state $|3\rangle$ corresponds to the lowest Stark level of the ${}^4I_{13/2}$ state.

decreases while the FWHM pulse duration increases. In general, the peak height is proportional to the square of the number of SR photons; thus, a decrease in peak height indicates a reduction in the SR photon number, which is consistent with this observation. This trend, where reduced SR photon number leads to a lower peak height and a broader pulse duration, is also in agreement with the characteristics of conventional SR.

3.1.3 Numerical simulation

To gain a quantitative understanding of this phenomenon, we perform numerical simulations aimed at reproducing the experimentally observed changes in periodic SR behavior induced by the trigger laser, with a particular focus on its power dependence.

Basic equations Previously, in Ref. [18], we constructed a model for periodic SR in the absence of the trigger laser. Here, we will apply such a model to consider the case where a trigger laser is added. The model we will construct is based on the Maxwell-Bloch equations for a reduced level system shown in Fig. 5, a pair of SR states plus a population reservoir state. The states $|1\rangle$ and $|2\rangle$ correspond to the lowest and the second lowest Stark levels of ${}^4I_{15/2}$ ground state, and $|3\rangle$ corresponds to the lowest Stark level of ${}^4I_{13/2}$ state, respectively. A single pumping rate P_{13} is used to represent both the excitation to the lowest Stark level of the ${}^4I_{9/2}$ state and subsequent nonradiative decay to $|3\rangle$. Among the various decay processes from $|3\rangle$, only the radiative decay rate A_{32} from $|3\rangle$ to $|2\rangle$ plays a role in SR. Coherence is assumed to develop only between these states. We collectively represent the other deexcitation processes from $|3\rangle$ that do not contribute to SR by the incoherent deexcitation rate A_{31} to $|1\rangle$. The ions in $|2\rangle$ return to $|1\rangle$ due to the nonradiative decay of the rate A_{21} .

By applying a rotating-wave and slowly varying envelope approximations to the Maxwell-

Bloch equations [20], the following set of equations can be derived.

$$\frac{d\rho_{11}}{dt} = -P_{13}\rho_{11} + A_{31}\rho_{33} + A_{21}\rho_{22}, \quad (2)$$

$$\frac{d\rho_{22}}{dt} = \Omega_s\rho_{32} + A_{32}\rho_{33} - A_{21}\rho_{22}, \quad (3)$$

$$\frac{d\rho_{33}}{dt} = -\Omega_s\rho_{32} + P_{13}\rho_{11} - (A_{31} + A_{32})\rho_{33}, \quad (4)$$

$$\frac{d\rho_{32}}{dt} = \frac{\Omega_s}{2}(\rho_{33} - \rho_{22}) - \gamma_{32}\rho_{32}, \quad (5)$$

$$\frac{\partial\Omega_s}{\partial t} = -\kappa\Omega_s + \Omega_0^2\rho_{32} + \Omega_0 R_{\text{sp}}\rho_{33} + \alpha\kappa_0\Omega_{\text{trig}}. \quad (6)$$

In this paper, we incorporate a new effect by the trigger laser into the last term of Eq. 6, which is introduced in Ref. [21]. The quantity Ω_{trig} is proportional to the trigger laser electric field E_{trig} . The coefficient α represents the degree of influence of the E_{trig} on SR. It is important to note that among the two quantities Ω_s and Ω_{trig} for the electric field in Eq. (6), Ω_s is the variable to be solved in the differential equations and Ω_{trig} is a constant input parameter. A detailed explanation of these equations, including parameters, is given in Appendix (A).

In our previous theoretical study [18], we introduced a dynamic modulation of the field decay rate κ to reproduce the experimentally observed periodic SR. Following the same approach, we again allow κ to switch between two values in response to the electric field, as described below.

$$\kappa(E_0) = \begin{cases} \kappa_0 & (|E_0| < E_{\text{th}}) \\ \kappa_0/q & (|E_0| > E_{\text{th}}), \end{cases} \quad (7)$$

where E_{th} is the threshold of the electric field. The parameter $q(> 1)$ quantifies the extent of the reduction in the field decay rate.

Simulation results In this section, we present numerical simulation results and compare them with the experimental results. The parameters used for simulations are introduced in Appendix (B). Figure 6 shows comparison of the trigger power dependence of (a) peak interval, (b) pulse area, (c) peak height, and (d) FWHM pulse duration between the experiment and simulation. The experimental data are shown as filled markers, consistent with Fig. 3, while the simulation results are shown as open markers. The leftmost points are the values without the trigger laser. Although the peak interval and FWHM duration can be directly compared, the pulse area and peak height are not directly comparable between the experimental and simulated results. Therefore, the experimental values are plotted on the left axis, and the simulation results on the right.

For the simulation, some of the parameters are adjusted to reproduce the experimental results. We use a parameter set $(P_{13}, A_{21}, A_{31}, A_{32}, \gamma_{32}) = (6, 2.5 \times 10^6, 104, 4, 10^8)$ Hz, $(q, E_{\text{th}}) = (2, 5 \times 10^{-6} \times (\sqrt{3}\hbar\Omega_0/d_{32}))$, and $\alpha = 3.8 \times 10^{-2}$. First of all, the pumping rate $P_{13} = 6$ Hz is adjusted to reproduce the experimental period in the absence of the trigger

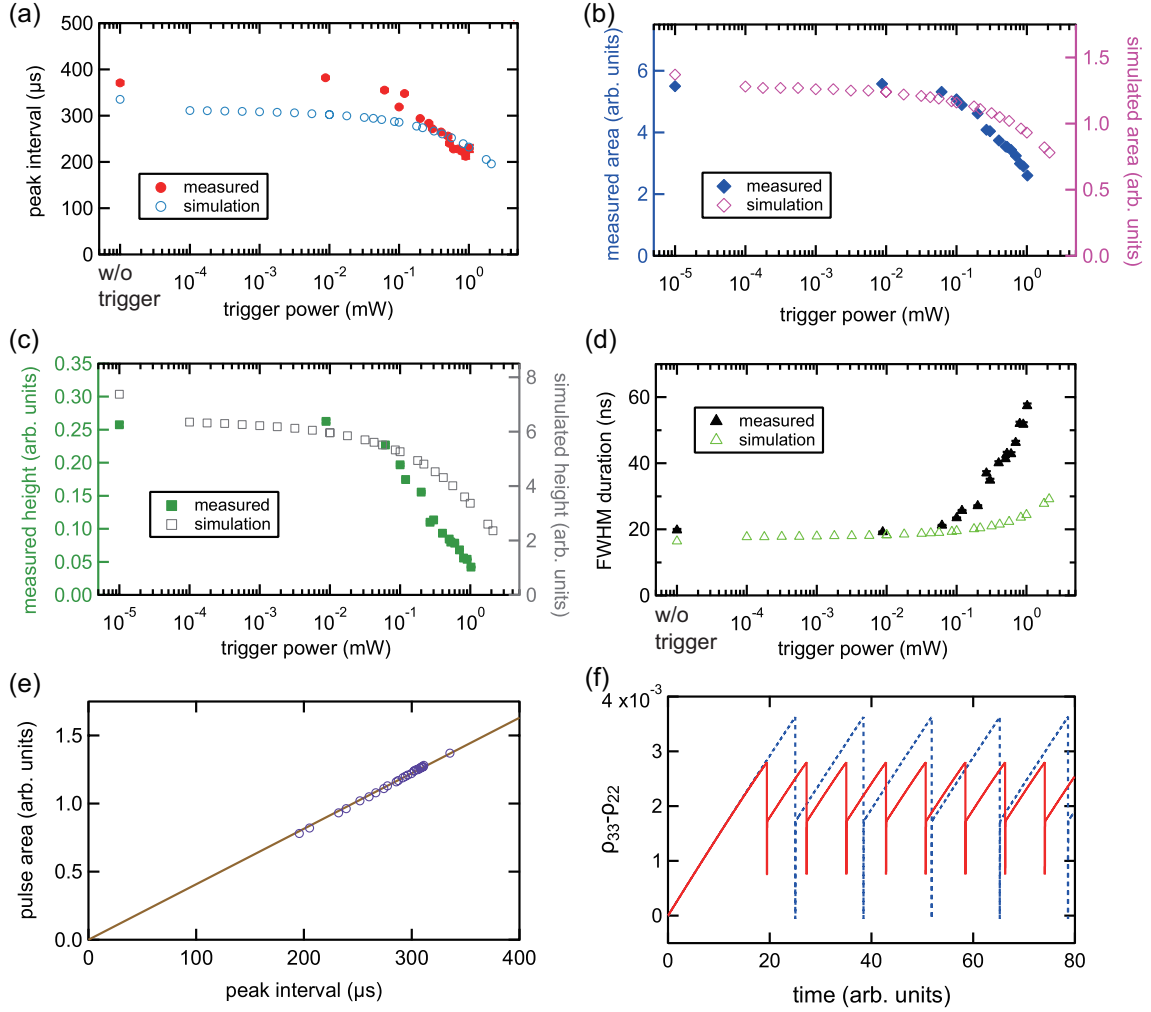


Figure 6: Comparison of the experimental results and numerical simulations. The experimental data are shown as filled markers, consistent with Fig. 3; the simulation results are shown as open markers. (a) Peak interval. (b) Pulse area. (c) Peak height. (d) FWHM pulse duration. The error bars in the experimental results are the standard errors. The leftmost points are the values without the trigger laser. Regarding the area and height of the SR pulses, the left axis corresponds to the experimental values and the right axis to the simulation results. (e) Pulse area plotted as a function of the period using the simulated values shown in (a) and (b). The solid line represents a linear fit constrained to pass through the origin. (f) Temporal evolution of population inversion ($\rho_{33} - \rho_{22}$) without (blue dashed) and with (red solid) trigger laser irradiation.

laser. When the actual value of 200 Hz is used in the simulation, the resulting period becomes more than an order of magnitude shorter than that observed experimentally. As mentioned in our previous paper [18], the effective value of P_{13} may reasonably be

lower if relaxation pathways bypassing $|3\rangle$ exist. Such pathways would reduce population accumulation and thus decrease the effective pumping rate to $|3\rangle$. The parameter $q = 2$ for κ modulation is taken from our previous study [18]. Varying the value of E_{th} has a small effect on the simulation results. However, both E_{th} and α need to be carefully adjusted to reproduce periodic SR, even under strong trigger laser conditions. The values of E_{th} and α used in this simulation were determined through iterative parameter tuning.

We closely examine the simulation results and compare them with experimental observations. Our simulation reproduces the decrease in the peak interval, pulse area, and pulse height with increasing trigger laser power, consistent with experiment. The absolute values obtained in both experiment and simulation are in good agreement. The FWHM duration increases with the strong trigger laser power, again consistent with the experiment. In the weak trigger power range, the trigger laser has a negligible effect. In the strong power range above a few mW, SR emission is not reproduced. While these overall trends agree reasonably well between experiment and simulation, the absolute value of the FWHM duration of SR pulses is larger in the experiment than in the simulation. The origin of this discrepancy remains unclear.

Similar to the experimental results, the period and pulse area in the simulation also show a proportional relationship as shown in Fig. 6 (e). The solid line is a linear fit constrained to pass through the origin. This proportional relationship can be understood by the constant excitation rate and the decrease of the threshold for SR generation. Figure 6 (f) shows temporal evolutions of population inversion ($\rho_{33} - \rho_{22}$) without (blue dashed) and with (red solid) trigger laser irradiation. The rate of increase in the population inversion is the same due to the same excitation rate. In the absence of the trigger laser, when the population inversion reaches a certain threshold, it rapidly decreases due to SR generation. Subsequently, the population inversion increases rapidly as ions in $|2\rangle$ deexcite to $|1\rangle$ with a lifetime of ~ 400 ns. The constant increase of the population inversion begins again due to the accumulation of $|3\rangle$ population. Our simulation shows that the threshold of SR generation decreases when the trigger laser is present. This result explains why both the period and pulse area decrease while maintaining a proportional relationship.

The influence of the trigger laser, quantified by the parameter α ($\sim 10^{-2}$), is very weak. This may be attributed to the limited spatial overlap between the SR mode and the trigger laser, since the propagation direction of SR differs from those of the excitation and trigger lasers despite optimized alignment of the trigger laser. Another possible reason is poor frequency mode matching between SR and the trigger laser. The trigger laser frequency cannot be adjusted with a precision better than approximately 100 MHz and its typical linewidth is on the order of 1 MHz, while the linewidth of SR is roughly 100 MHz, and individual SR pulses may have even narrower linewidths. As a result, the frequencies of SR and the trigger laser may not match exactly.

The κ modulation introduced in Ref. [18], derived from a theoretical model but not yet experimentally verified, yields reasonably accurate results. This result further supports the validity of employing dynamically varying parameters in modeling the system.

3.2 Trigger-enabled SR under optical excitation

We performed similar experiments under conditions where no SR is generated with the excitation laser alone. This condition could be achieved by changing the detuning of the excitation laser by 1 GHz. The change in laser detuning affects the excitation rate and decoherence due to crystal temperature, resulting in changes in the behavior of periodic SR. Under the achieved condition, the population inversion may not reach the SR threshold with the excitation laser alone, and a reduction of the threshold by the trigger laser is required. While the same time sequence as in Sec. 3.1 was used, the trigger laser power in this experiment was 9 mW. Figure 7 (a) shows an example of the observed waveform. The excitation laser is turned on for 40 ms from $t = 0$, and the trigger laser is turned on for 10 ms from $t = 15$ ms. As noted above, SR does not occur without the trigger laser. Periodic SR occurs only while the trigger laser is turned on. The inset shows the SR pulses around the onset of the trigger irradiation indicated by the gray dashed line at $t = 15$ ms. Strictly speaking, SR pulses do not occur immediately after the trigger pulse, but rather starts several tens of microseconds after the irradiation begins.

As an application of the above result, we considered that this system can be regarded as a device capable of generating SR pulses at desired timings. Based on this idea, we thought that the timing of SR generation might be controllable by short trigger laser irradiation, and performed the following experiment. The excitation laser is turned on for 40 ms from $t = 0$. The trigger laser with a duration of $33 \mu\text{s}$ is irradiated at the timing indicated by the dashed line in Fig. 7 (b) with a 6.7 ms period (150 Hz). Figure 7 (b) shows the probability of SR occurrence in $5 \mu\text{s}$. The trigger laser is irradiated six times during the 40 ms excitation. The first irradiation does not generate any SRs. It is likely because the excitation is insufficient and the population inversion has not yet reached the SR threshold. SRs occur between the first and second trigger irradiation, but the time of their occurrence varies widely. These SRs are generated even in the absence of the trigger laser. Even under experimental conditions nominally identical to those of Fig. 7 (a), SR between the first and second trigger pulses appeared in the condition of Fig. 7 (b), and the precise factors responsible for this behavior are not yet fully understood. For the second and subsequent irradiations, SRs occur immediately after the trigger laser irradiation.

The blue bars in Fig. 7 (c) represent the probability of occurrence of the “first” SR pulse in $5 \mu\text{s}$ for each trigger laser irradiation. The horizontal axis is the time after the trigger laser is turned on. The trigger laser is turned off at the dashed line ($t = 33 \mu\text{s}$). The rise and fall times of the trigger laser are typically around 100 ns and can be considered instantaneous switching in this plot. The data for the second to sixth irradiations in Fig. 7 (b) are used for this analysis. The same measurement was repeated 100 times, therefore each bar is the average probability for 500 trigger irradiations. The red line is the Gaussian fit. Interestingly, SR does not occur immediately after trigger laser irradiation; instead, the first SR pulse is generated on average $82 \mu\text{s}$ after the trigger, with a standard deviation of $15 \mu\text{s}$. This result indicates that, although it is not possible to synchronize SR generation exactly with the trigger, its timing can be

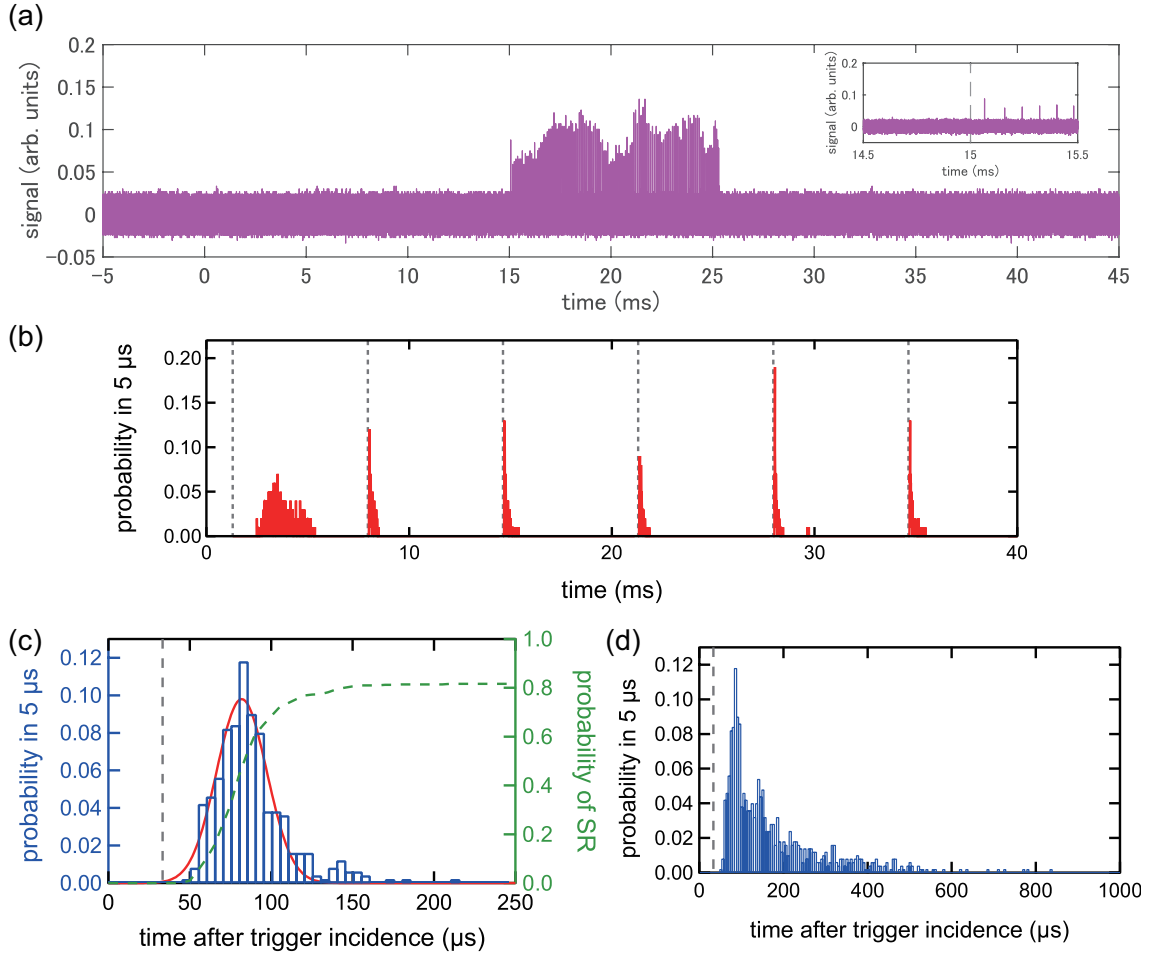


Figure 7: (a) Example waveform of observed periodic SR pulses. The excitation laser is turned on for 40 ms from $t = 0$, and the trigger laser is turned on for 10 ms from $t = 15$ ms. No SR is generated in the absence of the trigger laser. The inset is an enlarged view of the SR pulse behavior around the onset of the trigger irradiation (gray dashed line at $t = 15$ ms). (b) Probability of SR occurrence within $5 \mu\text{s}$ intervals. The trigger laser, with a duration of $33 \mu\text{s}$, is applied at the timing indicated by the dashed lines. (c) Probability (in $5 \mu\text{s}$ bins) of the timing of the first SR pulse for each trigger laser irradiation. The blue bars (left axis) represent the measured data, and the red line shows a Gaussian fit. The green dashed line (right axis) represents the cumulative of the blue bars. (d) Probability (in $5 \mu\text{s}$ bins) of the timing of the all SR pulse for each trigger laser irradiation.

controlled with a precision corresponding to a standard deviation of $15 \mu\text{s}$. As can be seen, SR tends to occur more prominently after the trigger laser is turned off. This behavior may be related to improved coherence in the absence of laser-induced heating of the crystal. Alternatively, stimulated emission during the trigger irradiation could reduce

the population of the upper SR state, thereby preventing the system from reaching the SR threshold. However, the underlying mechanism responsible for this tendency remains unclear. The green dashed line represents the cumulative sum of the probabilities shown by the blue bars. This system can be regarded as a device that generates SR pulses with an 80 % probability in response to trigger irradiation. This probability increases with stronger or longer trigger laser irradiation.

On the other hand, there is no strict one-to-one correspondence between the trigger laser and the SR pulse; multiple SR pulses are generated for each trigger irradiation. Figure 7 (d) shows the probability of occurrence of the “all” SR pulses in 5 μs for each trigger. After the trigger irradiation, the probability of SR reaches its peak at approximately 80 μs . Subsequently, the SR probability gradually decreases, and by around 600 μs , it becomes almost negligible. A small secondary peak appears at about 140 μs , which is considered to correspond to the second burst of periodic SR following the first peak. See Appendix (E) for more details.

4 Summary

To achieve more controllable coherence development, we investigated the effects of a trigger laser on periodic SR. As expected from conventional triggered SR, both the period and its variance decreased upon irradiation with the trigger laser, indicating enhanced controllability of coherence development. In measurements of trigger power dependence, although both the period and the number of SR photons decrease with increasing the trigger laser power, they remain proportional to each other. This behavior can be understood by the decrease in the SR threshold under the constant excitation rate, which was also confirmed by numerical simulations. The fact that the field decay rate modulation introduced in Ref. [18] is also effective in the presence of a trigger laser supports the validity of our model. Furthermore, we successfully generated SR using the trigger laser in situations where periodic SR does not occur with an excitation laser alone. This technique allowed us to control the timing of SR generation through irradiation with a short trigger laser pulse and yielded a device capable of generating SR pulses at desired timing. Triggered periodic SR presents potential as a light source that generates narrow linewidth optical pulses at nearly constant intervals composed of a cooled crystal and two CW lasers. The ability to control and stabilize the periodicity of SR pulses may enable applications in quantum information processing, quantum sensing, and fundamental physics, where additional manipulation can be performed by utilizing a maximum coherence.

Acknowledgments

This work was supported by JSPS KAKENHI (Grants No. JP19H00686, No. JP20H00161, No. JP21H01112, No. JP25K00940, JP25K01027, and JP25K07337) and the Korea Research Foundation (Grant No. 2020R1A2C3009299).

Appendix

(A) Detailed explanation of equations for numerical simulation

In the main text, the following set of equations are used for numerical simulation.

$$\frac{d\rho_{11}}{dt} = -P_{13}\rho_{11} + A_{31}\rho_{33} + A_{21}\rho_{22}, \quad (2)$$

$$\frac{d\rho_{22}}{dt} = \Omega_s\rho_{32} + A_{32}\rho_{33} - A_{21}\rho_{22}, \quad (3)$$

$$\frac{d\rho_{33}}{dt} = -\Omega_s\rho_{32} + P_{13}\rho_{11} - (A_{31} + A_{32})\rho_{33}, \quad (4)$$

$$\frac{d\rho_{32}}{dt} = \frac{\Omega_s}{2}(\rho_{33} - \rho_{22}) - \gamma_{32}\rho_{32}, \quad (5)$$

$$\frac{\partial\Omega_s}{\partial t} = -\kappa\Omega_s + \Omega_0^2\rho_{32} + \Omega_0 R_{\text{sp}}\rho_{33} + \alpha\kappa_0\Omega_{\text{trig}}. \quad (6)$$

A detailed explanation of these equations is given below. Here, ρ_{ij} are the density matrix elements of $|i\rangle$ and $|j\rangle$. The Rabi frequency is defined as $\Omega_s \equiv id_{32}E_0/\sqrt{3}\hbar$, where d_{32} is the transition dipole moment between $|3\rangle$ and $|2\rangle$, and E_0 is the slowly varying envelope of the electric field due to the SR radiation. Equation (5) describes the temporal evolution of the coherence, including decoherence at the rate γ_{32} . Equation (6), derived from the Maxwell equation, describes the time evolution of the SR electric field. The emission of SR radiation from the crystal is characterized by a field decay rate $\kappa = \kappa_0 \equiv c/n_0L$, where c is the speed of light and $n_0 = 1.8$ is the refractive index of the crystal at the SR wavelength. We call R_{sp} the coherence trigger rate, which represents the contribution of spontaneous emission to the SR electric field. The frequency Ω_0 , defined as $\Omega_0 \equiv \sqrt{N_0 d_{32}^2 \omega_{32} / 3\epsilon_0 \hbar}$, characterizes the time scale of the system. Here N_0 is the number density of Er^{3+} ions at site 2 and ω_{32} is the angular frequency between $|3\rangle$ and $|2\rangle$. A new effect by the trigger laser is incorporated into the last term of Eq. 6. The quantity Ω_{trig} is proportional to the trigger laser electric field E_{trig} , defined as $\Omega_{\text{trig}} \equiv id_{32}E_{\text{trig}}/\sqrt{3}\hbar$. The coefficient α represents the degree of influence of E_{trig} on SR. There are several factors that determine α , one of which is the spatial overlap between the excitation and trigger lasers. In an ideal case, $\alpha = 1$. Let us consider the case in which the incident trigger laser passes through the crystal without interacting with any ions. In this situation, the time derivative on the left-hand side, as well as the second and third terms on the right-hand side of the equation, become zero. As a result, the Ω_s becomes equal to Ω_{trig} . It also becomes evident that the coefficient of Ω_{trig} is $+\kappa_0$ [21].

(B) Parameters in simulations

We briefly introduce the parameters used in the simulation. They are summarized in Table 1. The upper part is related to the rates. The actual values and measure of uncertainties are same as those in Ref. [18]. The lower part shows the parameters related to the trigger irradiation and κ modulation. The right column shows the values used in

Table 1: Simulation parameters. The upper part is related to the rates. The lower part shows the parameters related to the trigger laser irradiation and κ modulation. Here, the uncertainty does not mean 1σ , but is only a guide. “factor U ” represents the uncertainty from factor $1/U$ to U .

symbol	actual value	measure of uncertainty	values used in this paper
P_{13}	200 Hz	± 100 Hz	6 Hz
A_{32}	4 Hz	factor 10	4 Hz
A_{31}	100 Hz	$70 \leq A_{31} \leq 110$ Hz	104 Hz
A_{21}	2.5×10^6 Hz	factor 3	2.5×10^6 Hz
γ_{32}	10^7 Hz	factor 10	10^8 Hz
R_{sp}			$10^{-30} \times \Omega_0$
α			3.8×10^{-2}
q			2
E_{th}			$5 \times 10^{-6} \times (\sqrt{3}\hbar\Omega_0/d_{32})$

this simulation. The value of γ_{32} is adjusted within the uncertainty range while P_{13} is adjusted beyond the uncertainty range so that the period in the absence of the trigger laser is comparable to the experimental value. This adjustment can be justified by the consideration of other relaxation pathways bypassing $|3\rangle$. The quantity q is the same as that in Ref. [18]. The values of α and E_{th} are chosen through trial and error, as described in Sec. 3.1.3. In the numerical simulation, the dependence of each parameter, such as period, is investigated by changing the trigger laser power P_{trig} . Ω_{trig} , as a function of P_{trig} , is evaluated from the relation $I_{\text{trig}} = \frac{1}{2}c\epsilon_0|E_{\text{trig}}|^2$ with the trigger laser intensity I_{trig} . For simplicity, we assume a flat beam of radius w_0 instead of a Gaussian beam when determining I_{trig} .

(C) Trigger frequency dependence

In the main text, we focus on how the trigger laser influences the SR period. In Appendix (C) and (D), we present additional properties of periodic SR. The results shown below were obtained under the experimental condition described in Sec. 3.1.

We varied the trigger laser frequency to investigate how wide the frequency range affects the behavior of periodic SR. Figure 8 (a) shows the resulting dependence of the peak interval on the trigger laser frequency. Within the 100 MHz range, the peak interval is consistently shorter than that in the absence of a trigger laser. This width is much narrower than the typical inhomogeneous broadening in this crystal (~ 1 GHz) and is comparable to the linewidth of SR measured in our experiment [17]. The frequency in Fig. 8 (a) is around the SR transition, but absolute zero-detuning point (*i.e.* exact resonance condition) remains uncertain due to the wavemeter accuracy (WS6-200IR II; HighFinesse, absolute accuracy 120 MHz). The effective trigger frequency range of

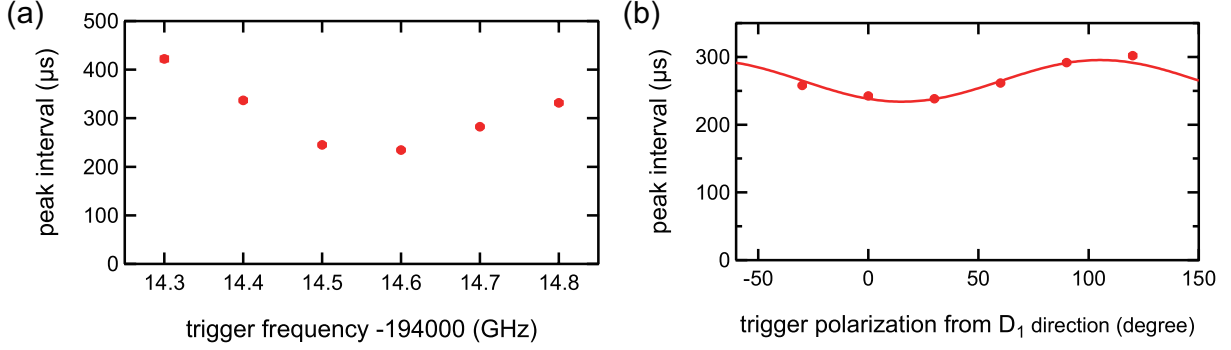


Figure 8: (a) Dependence of peak interval on the trigger laser frequency. The red circles and error bars represent the averages and standard errors, respectively. (b) Dependence of peak interval on the trigger laser polarization. The horizontal axis is the angle of the trigger laser polarization from the \mathbf{D}_1 axis. The red circles and error bars represent the averages and standard errors, respectively. The solid line is the fit by a sine function with a fixed period of 180° .

approximately 100 MHz is consistent with the intuitive expectation that the influence on periodic SR is maximized when the trigger frequency matches the SR frequency.

(D) Trigger polarization dependence

We investigated the influence of trigger laser polarization on the periodic SR behavior. Figure 8 (b) shows the dependence of the peak interval on the polarization angle of the trigger laser. The horizontal axis represents the angle from the \mathbf{D}_1 axis, which is approximately aligned with SR polarization in the absence of the trigger laser. The red circles and error bars indicate the average values and standard errors, respectively. The results show that the peak interval becomes shortest when the trigger laser polarization is parallel to the SR polarization. Conversely, the effect on the periodic SR is reduced when the trigger laser polarization is orthogonal to the SR polarization. This polarization dependence is consistent with physical expectations. The solid line represents a sine-function fit with a fixed period of 180° . The angle at which the minimum peak interval occurs is approximately $+15^\circ$. The polarization of the SR is also tilted by a similar angle, and the most effective trigger polarization nearly coincides with the SR polarization. There is no particular reason to expect that the SR polarization should be strictly aligned with the \mathbf{D}_1 axis. The $+15^\circ$ deviation may include a contribution from a slight misalignment of the \mathbf{D}_1 axis relative to the vertical direction due to the mounting of the crystal in the copper holder.

The dependence of the period on the trigger laser polarization under the experimental condition described in Sec. 3.1 is consistent with intuition. In contrast, under the conditions in Sec. 3.2, SR pulses are generated regardless of the trigger laser polarization, even though no SR is generated with the excitation laser alone. In this case, the polarization of the SR pulses is also parallel to the \mathbf{D}_1 axis. Such experimental observations, which

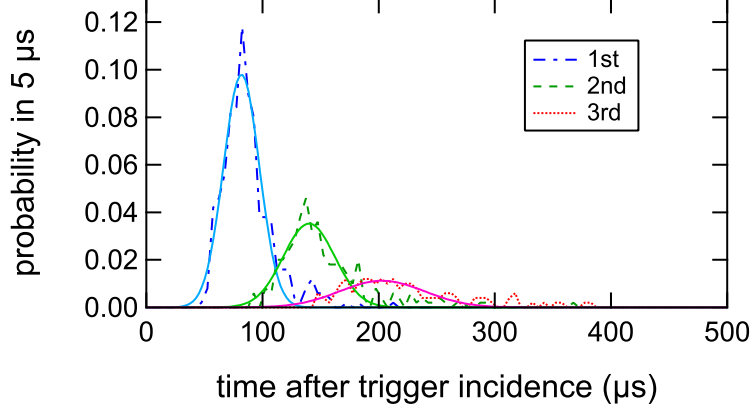


Figure 9: Probabilities (in $5 \mu s$ bins) of the timing of the first (blue dot-dashed line), second (green dashed line), and third (red dotted line) SR pulses for each trigger irradiation. The blue dot-dashed line is consistent with Fig. 7 (e). The cyan, lightgreen, and magenta lines are Gaussian fits.

are counterintuitive with respect to the polarization of the trigger laser and SR pulses, are not taken into account in the simulations presented in Sec. 3.1.3. The underlying mechanism responsible for this counterintuitive behavior remains unclear and will be the subject of future investigation.

(E) Multiple SR pulses for Short Trigger Irradiation

Regarding the short trigger experiment in Sec. 3.2, we noted that there is no strict one-to-one correspondence between the trigger laser and the SR pulse; multiple SR pulses are generated for each trigger irradiation. Figure 7 (d) shows the probability of occurrence of the “all” SR pulses in $5 \mu s$ for each trigger. Approximately $80 \mu s$ after the trigger irradiation, the probability of SR occurrence reaches its peak and then gradually decreases. A small secondary peak appearing at about $140 \mu s$ corresponds to the second burst of periodic SR following the first peak. Figure 9 shows the probability distributions of the timing of the first, second, and third SR pulses for each trigger irradiation. The cyan, lightgreen, and magenta lines are Gaussian fits for the corresponding SR pulses. It can be seen that the probability of the second SR pulse reaches its maximum at around $140 \mu s$. For the second and third SR pulses, the probability of SR occurrence decreases and the temporal fluctuation of the emission timing becomes larger. The probability of the third SR pulse peaks at around $200 \mu s$. These SR pulses are generated with an average period of approximately $60 \mu s$. The first SR pulse exhibits the smallest timing variation and is therefore the most precisely controlled. Note that the SR pulses continue beyond the fourth emission, but these subsequent pulses are not shown in Fig. 9.

References

- [1] R. H. Dicke, “Coherence in spontaneous radiation processes,” *Phys. Rev.* **93** (Jan, 1954) 99–110.
- [2] N. Skribanowitz, I. P. Herman, J. C. MacGillivray, and M. S. Feld, “Observation of dicke superradiance in optically pumped hf gas,” *Phys. Rev. Lett.* **30** (Feb, 1973) 309–312.
- [3] M. Gross, C. Fabre, P. Pillet, and S. Haroche, “Observation of near-infrared dicke superradiance on cascading transitions in atomic sodium,” *Phys. Rev. Lett.* **36** (Apr, 1976) 1035–1038.
- [4] R. Florian, L. Schwan, and D. Schmid, “Superradiance and high-gain mirrorless laser activity of O_2^- -centers in KCl,” *Solid State Communications* **42** no. 1, (1982) 55–57.
- [5] K. Cong, Q. Zhang, Y. Wang, G. T. Noe, A. Belyanin, and J. Kono, “Dicke superradiance in solids,” *J. Opt. Soc. Am. B* **33** no. 7, (Jul, 2016) C80–C101.
- [6] G. Rainò, M. A. Becker, M. I. Bodnarchuk, R. F. Mahrt, M. V. Kovalenko, and T. Stöferle, “Superfluorescence from lead halide perovskite quantum dot superlattices,” *Nature* **563** no. 7733, (2018) 671–675.
- [7] A. Angerer, K. Streltsov, T. Astner, S. Putz, H. Sumiya, S. Onoda, J. Isoya, W. J. Munro, K. Nemoto, J. Schmiedmayer, *et al.*, “Superradiant emission from colour centres in diamond,” *Nature Physics* **14** no. 12, (2018) 1168–1172.
- [8] J. Kim, D. Yang, S. hoon Oh, and K. An, “Coherent single-atom superradiance,” *Science* **359** no. 6376, (2018) 662–666.
- [9] C. Braggio, F. Chiossi, G. Carugno, A. Ortolan, and G. Ruoso, “Spontaneous formation of a macroscopically extended coherent state,” *Phys. Rev. Research* **2** (Jul, 2020) 033059.
- [10] F. Chiossi, C. Braggio, A. Khanbekyan, G. Carugno, A. Ortolan, G. Ruoso, R. Calabrese, A. Di Lieto, L. Tomassetti, and M. Tonelli, “Cascade superfluorescence in Er:YLF,” *Phys. Rev. Res.* **3** (Feb, 2021) 013138.
- [11] K. Kitano and H. Maeda, “Coherent amplification of continuous laser field via superfluorescence,” *Phys. Rev. Lett.* **132** (Feb, 2024) 073201.
- [12] Q. H. F. Vrehen and M. F. H. Schuurmans, “Direct measurement of the effective initial tipping angle in superfluorescence,” *Phys. Rev. Lett.* **42** (Jan, 1979) 224–227.

- [13] W. Kersten, N. de Zordo, O. Diekmann, T. Reiter, M. Zens, A. N. Kanagin, S. Rotter, J. Schmiedmayer, and A. Angerer, “Triggered superradiance and spin inversion storage in a hybrid quantum system,” *Phys. Rev. Lett.* **131** (Jul, 2023) 043601.
- [14] N. Carlson, D. Jackson, A. Schawlow, M. Gross, and S. Haroche, “Superradiance triggering spectroscopy,” *Optics Communications* **32** no. 2, (1980) 350–354.
- [15] M. Houde, F. Rajabi, B. M. Gaensler, A. Mathews, and V. Tranchant, “Triggered superradiance and fast radio bursts,” *Monthly Notices of the Royal Astronomical Society* **482** no. 4, (11, 2018) 5492–5499.
- [16] L. Hao, Z. Bai, J. Bai, S. Bai, Y. Jiao, G. Huang, J. Zhao, W. Li, and S. Jia, “Observation of blackbody radiation enhanced superradiance in ultracold Rydberg gases,” *New Journal of Physics* **23** no. 8, (2021) 083017.
- [17] H. Hara, J. Han, Y. Imai, N. Sasao, A. Yoshimi, K. Yoshimura, M. Yoshimura, and Y. Miyamoto, “Periodic superradiance in an Er:YSO crystal,” *Physical Review Research* **6** (2024) 013005.
- [18] H. Hara, Y. Miyamoto, J. Han, R. Omoto, Y. Imai, A. Yoshimi, K. Yoshimura, M. Yoshimura, and N. Sasao, “Analytical and numerical studies of periodic superradiance,” *Phys. Rev. A* (Feb, 2026) . accepted for publication.
- [19] R. Bonifacio and L. A. Lugiato, “Cooperative radiation processes in two-level systems: Superfluorescence,” *Phys. Rev. A* **11** (May, 1975) 1507–1521.
- [20] M. Benedict, A. Ermolaev, V. Malyshev, I. Sokolov, and E. Trifonov, *Super-radiance: Multiatomic Coherent Emission*. CRC Press, 1996.
- [21] P. Goy, L. Moi, M. Gross, J. M. Raimond, C. Fabre, and S. Haroche, “Rydberg-atom masers. II. Triggering by external radiation and application to millimeter-wave detectors,” *Phys. Rev. A* **27** (Apr, 1983) 2065–2081.